International Journal of Heat and Fluid Flow 30 (2009) 99–107

Contents lists available at ScienceDirect

International Journal of Heat and Fluid Flow

journal homepage: www.elsevier.com/locate/ijhff

Atomized non-equilibrium two-phase flow in mesochannels: Momentum analysis

John D. Schwarzkopf, Clayton T. Crowe, Prashanta Dutta *, Ben Q. Li

School of Mechanical and Materials Engineering, Washington State University, Pullman, WA 99164-2920, United States

ARTICLE INFO

Article history:
Received 12 June 2008
Received in revised form 23 September 2008
Accepted 25 September 2008
Available online 13 November 2008

Keywords:
Boiling
Two-phase flow
Spray droplet
Mesochannel
Electronic cooling

ABSTRACT

Two-phase pressure drop measurements are very difficult to make while the fluid is in non-equilibrium condition, i.e. while phase change is taking place. This is further complicated when an atomized liquid is introduced in the system at much higher velocity than other components such as liquid layer, vapor core, and entrained droplets. The purpose of this paper is to develop a model to predict the two-phase pressure characteristics in a mesochannel under various heat flux and liquid atomization conditions. This model includes the momentum effects of liquid droplets from entrainment and atomization. To verify the model, an in-house experimental setup consisting of a series of converging mesochannels, an atomization facility and a heat source was developed. The two-phase pressure of boiling PF5050 was measured along the wall of a mesochannel. The one-dimensional model shows good agreement with the experimental data. The effects of channel wall angle, droplet velocity and spray mass fraction on two-phase pressure characteristics are predicted. Numerical results show that an optimal spray cooling unit can be designed by optimizing channel wall angle and droplet velocity.

1. Introduction

Air cooled heat sinks are generally used to remove heat from electronic devices because of the level of reliability and low cost. But in the last decade the frequency of the central processing unit (CPU) has increased dramatically, thereby increasing the level of heat dissipation. Cader and Tilton (2004) compared the change in processing performance of an air cooled Intel Xeon 3.0 GHz microprocessor packaged in a 1U server (4.45 cm height) while varying the ambient temperature. The results show that the performance of the air cooled processor dropped nearly 30% when operating in a 40 °C environment. The air cooled configuration showed significant throttling of the processor computing ability as the ambient temperature rose above 27 °C. For commercial applications, air cooled heat sinks could be an acceptable solution in temperature controlled clean rooms, but for military applications, this is very problematic considering that such systems have to operate in an ambient temperature as high as 60 °C. In order to minimize the throttling effect at high ambient temperatures, the package size of the air cooled heat sink must be increased by 2–3 folds. Conversely, a data center with air cooled heat sinks would have to reduce its data processing capability by 2–3 times per unit volume. As electronic packaging becomes dense and power densities continue to rise, a need for an alternative cooling solution is apparent.

In the electronic cooling industry, two-phase flows are well recognized for their superior heat transfer and increased heat removal limits. Various two-phase mechanisms tested for electronic cooling are pool boiling, convective flow boiling, and spray cooling (Chu et al., 2004). Among them spray cooling has shown to be effective at cooling very high heat flux components in dense electronic packaging where an order of magnitude increase in heat transfer coefficient and critical heat flux can be obtained over conventional pool boiling (Rini et al., 2001, 2002). The term "spray cooling" involves a range of atomization techniques (such as full cone, hollow cone, or pulsed) but traditionally implies that a thin film of liquid is maintained at the surface to absorb the heat. In a spray cooling system, the heat acquisition process involves the combined effects of convection, boiling, and evaporation (Rini et al., 2002). The droplet and vapor momentum dictate the liquid film thickness at the surface, thus controlling heat transfer performance. A qualitative trend of spray cooling vs. pool boiling performance is shown in Fig. 1. Although spray cooling has much higher heat removal ability over pool boiling techniques (Rini et al., 2001), this performance improvement is typically associated with small (<1.5 cm × 1.5 cm) heat acquisition areas (Tilton, 1989; Mudawar and Estes, 1996; Rini et al., 2002). When cooling large areas with high heat loads, spray cooling performance usually decreases (i) due to difficulties in managing the flow of multiple atomizers and (ii) due to the increased spray distance needed to provide adequate fluid coverage (Schwarzkopf, 2005). One can eliminate these drawbacks of spray cooling while retaining good heat transfer by designing a system with an array of mesochannels, shown in Fig. 2 and described elsewhere (Schwarzkopf et al., 2005). In this system, liquid is atomized

* Corresponding author. Tel.: +1 509 335 7989; fax: +1 509 335 4662.
E-mail address: dutta@mail.wsu.edu (P. Dutta).

0142-727X/$ - see front matter © 2008 Elsevier Inc. All rights reserved.
doi:10.1016/j.ijheatfluidflow.2008.09.007

Nomenclature

A	cross-sectional area [m^2]
C	droplet concentration
D	diameter [m]
D_t	tube diameter [m]
E	entrained droplet liquid mass fraction
F	force [N]
f	drag factor
g	acceleration due to gravity [m/s^2]
G	mass flux [kg/m^2]
G_{lfo}	minimum liquid film mass flux at which entrainment will occur [kg/m^2]
k_d	entrained droplet deposition coefficient
$\dot{m}$	mass flow rate [kg/s]
N	number of droplets
p	pressure [N/m^2]
S	spray droplet liquid mass fraction
U	velocity of a component [m/s]
x	quality
X	Martinelli factor
z	coordinate system along the flow
$\overline{()}$	average of variable ( )

Greek symbols

α	void or vapor phase volume fraction
β	liquid layer volume fraction
χ	upper wall angle [°]
δ	lower wall angle [°]
ϕ	two-phase multiplier
Φ	angle between flow axis and horizontal [°]
η	entrained droplet volume fraction
κ	spray droplet volume fraction
μ	dynamic viscosity [$N\,s/m^2$]
ρ	density [kg/m^3]
σ	surface tension [N/m]
τ	response time [s]
$\forall$	volume [m^3]

Subscripts

dep	deposited
ed	entrained droplet
ent	entrained
fr	related to friction
i	liquid–vapor interface
l	liquid phase
ll	liquid layer
lv	liquid–vapor
$l \rightarrow i$	at liquid–vapor interface
$l \rightarrow w$	at liquid–wall interface
sd	spray droplet
t	tube
tt	turbulent-liquid–turbulent-vapor
v	vapor phase
$v \rightarrow i$	at vapor–liquid interface
$v \rightarrow w$	at vapor–wall interface
w	wall

and the high velocity droplets pump the surrounding vapor to create an initial quality at the onset of the channel. The purpose of the initial quality is to promote annular flow throughout the length of the channel, resulting in increased heat transfer (Schwarzkopf, 2005). According to the Chen correlation (1966), two-phase heat transfer coefficients in the annular regime are higher than those in the liquid, bubbly or slug regimes (Schwarzkopf et al., 2005; Schwarzkopf, 2005). Thus the method described above (to create an initial quality, as shown in Fig. 2) is proposed to obtain a thin film of liquid along the wall, promoting annular flow at the beginning of the channel and thereby increasing the heat transfer coefficient throughout the channel relative to traditional flow boiling practices. However, in order to achieve this, the pressure drop in the channel must be understood.

In the event of pumping vapor, by means of an atomization process, into a channel in which boiling occurs, the vapor momentum flux at the inlet boundary of the channel should be balanced with the pressure drop across the channel (Schwarzkopf, 2005). If the entrained vapor does not have enough momentum flux to overcome the pressure drop, the high pressure region will shift downstream in the channel and force a portion of the vapor to flow in the opposite direction of the sprayed droplets which can result in pressure oscillations and premature dry out. A numerical study shows that the droplet momentum flux is typically an order of magnitude greater than the vapor momentum flux (Schwarzkopf, 2005). Hence, the droplets can continue wetting the channels even if vapor flow reversal is present but the thermal performance should be reduced by such an action.

Understanding and predicting the trends in pressure distribution associated with a given mass flow rate is crucial to utilizing the heat transfer performance gained by an initial quality. The traditional approach to determine the two-phase pressure drop involves utilization of correlations derived from homogeneous or separated flow theory (Carey, 1992), both of which do not include effects of atomized droplet momentum. Carey (1992) derived a two-phase pressure drop correlation independently for both the liquid and vapor phases and sums them together to form a mixture equation. However, he did not consider the momentum effect of spray droplets and entrained droplets. The system of interest (referred to as a spray module, Schwarzkopf et al., 2005) includes

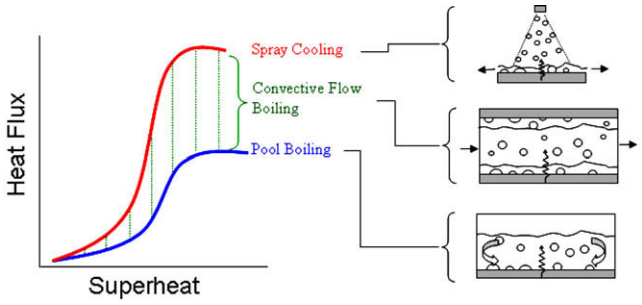

Fig. 1. Generic heat flux curves for various boiling concepts.

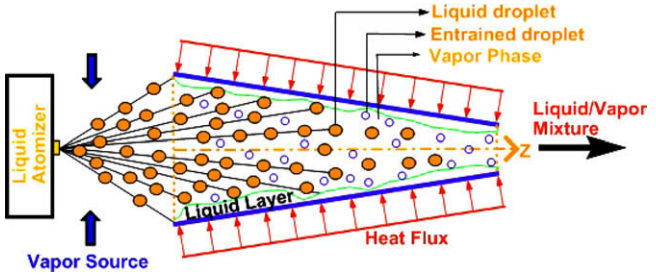

Fig. 2. Fundamental concept of heat transfer augmentation in a mesochannel by introducing an initial quality through spray droplets. An array of mesochannels can be used to reject heat from a large area.

spray and entrained droplets. The spray droplets are formed by an atomization process and the entrained droplets are formed by the turbulent interaction at the surface of the liquid/vapor interface. In this study, a pressure drop equation for two-phase flow in a mesochannel involving (a) vapor core in the center, (b) liquid layer on the wall, (c) spray droplets within the vapor core, and (d) entrained droplets from the liquid layer to the vapor core is derived from fundamentals. The purpose of this study is to understand the pressure drop within a mesochannel during the presence of boiling.

2. Mathematical modeling

Modeling of two-phase flow is a complicated task; thus a simple quasi-one-dimensional approach was developed to predict the magnitude and trend of the two-phase momentum in a channel with increasing quality. A control volume of the liquid/vapor mixture, along with their interactions, is shown in Fig. 3. The mixture contains spray droplets, entrained droplets, a liquid layer on the wall and a vapor core in the center of the channel. The fluid was divided into these four components to account for momentum effects due to velocity differences between the components. For instance, the velocity of the atomized droplets can be higher than the vapor, thus acting as a pump by transferring momentum to the vapor. However, the entrained droplets are assumed to leave the liquid layer at the velocity of the liquid layer which is considered to be lower than the velocity of the vapor. When coupled, these effects can cause the change in momentum to be much different than that of a single phase fluid.

A quasi-one-dimensional analysis can be used by assuming that the transition in area is gradual such that no separation occurs (Crowe et al., 1998). The other assumptions in deriving the fundamental mixture momentum equations are listed as follows:

1. There is no mass transfer between the droplets and the vapor.
2. The velocity of the vapor generated at the wall is equal to the liquid layer velocity.
3. Liquid and gas phase velocities are uniform across the cross-sectional area occupied by each component. The velocities of each component are not assumed to be equivalent and vary only in the direction of flow.
4. Steady state conditions.

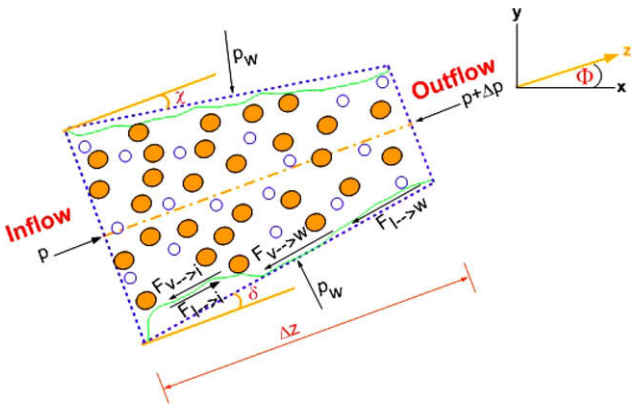

Fig. 3. Schematic of a control volume depicting various forces acting on different components in a non-equilibrium two-phase flow. Four components considered in this momentum study are vapor core in the center, liquid layer on the wall, spray droplets within the vapor core, and entrained droplets from the liquid layer to the vapor core. The spray droplets are formed by the atomization process, the entrained droplets are generated by the turbulent interaction at the liquid/vapor interface, the liquid layer is formed by the atomized droplets hitting the wall, and the vapor is initially pumped into the channel and generated within the channel by the boiling.

3. Development of model equations

For a pseudo one-dimensional geometry, the summation of the forces acting on the vapor layer, liquid layer, spray droplets and entrained droplets can be expressed as

$$\sum F_v = -\Delta(pA_v) + \overline{p}\Delta A_v - F_{v\to w} - F_{v\to i} - 3\pi N_{sd}\mu_v D_{sd} f_{sd}(\overline{U}_v - \overline{U}_{sd}) - 3\pi N_{ed}\mu_v D_{ed} f_{ed}(\overline{U}_v - \overline{U}_{ed}) - \forall_v \rho_v g\sin(\Phi) \quad (1)$$

$$\sum F_{ll} = -\Delta(pA_{ll}) + \overline{p}\Delta A_{ll} - F_{l\to w} - F_{l\to i} - \forall_{ll}\rho_l g\sin(\Phi) \quad (2)$$

$$\sum F_{sd} = -3\pi N_{sd}\mu_v D_{sd} f_{sd}(\overline{U}_{sd} - \overline{U}_v) - N_{sd}\overline{\forall}_{sd}\frac{dp}{dz} - N_{sd}\overline{\forall}_{sd}\rho_l g\sin(\Phi) \quad (3)$$

$$\sum F_{ed} = -3\pi N_{ed}\mu_v D_{ed} f_{ed}(\overline{U}_{ed} - \overline{U}_v) - N_{ed}\overline{\forall}_{ed}\frac{dp}{dz} - N_{ed}\overline{\forall}_{ed}\rho_l g\sin(\Phi) \quad (4)$$

According to Newton's second law of motion, the forces are balanced by the rate of change of momentum. For each component, the rate of change of momentum depends on the momentum inflow, outflow and storage rate (shown in Table 1). These terms are discussed in the following sections.

3.1. Steady state one-dimensional vapor phase momentum equation

The rate of change of momentum of the vapor phase must account for the mass and momentum transfer due to boiling action. To simplify the analysis, it is assumed that the vapor generated within the liquid layer enters the vapor control volume at the average liquid velocity. With this assumption, the rate of change of momentum in the vapor phase across the control volume can be expressed as

$$\sum F_v = \dot{m}_v U_v + \frac{d}{dz}(\dot{m}_v U_v)\Delta z - \dot{m}_{lv}\overline{U}_{ll} - \dot{m}_v U_v \quad (5)$$

Equating Eqs. (1) and (5) reveals a momentum equation for the vapor core

$$-\Delta(pA_v) + \overline{p}\Delta A_v - F_{v\to w} - F_{v\to i} - 3\pi N_{sd}\mu_v D_{sd} f_{sd}(\overline{U}_v - \overline{U}_{sd}) - 3\pi N_{ed}\mu_v D_{ed} f_{ed}(\overline{U}_v - \overline{U}_{ed}) - \forall_v \rho_v g\sin(\Phi) = \frac{d}{dz}(\dot{m}_v U_v)\Delta z - \dot{m}_{lv}\overline{U}_{ll} \quad (6)$$

The volume of vapor can be expressed as $\forall_v = A_v\Delta z = \alpha A\Delta z$. The number of spray droplets (N_{sd}) and the number of entrained droplets (N_{ed}) can be written in terms of a mean droplet diameter, $N_{sd} = \frac{\kappa A\Delta z}{\frac{\pi}{6}D_{sd}^3}$ and $N_{ed} = \frac{\eta A\Delta z}{\frac{\pi}{6}D_{ed}^3}$. With these formulations, the following equation is obtained:

$$-\Delta(p\alpha A) + \overline{p}\Delta(\alpha A) - F_{v\to w} - F_{v\to i} - \rho_l \kappa A\frac{f_{sd}}{\tau_{sd}}\Delta z(\overline{U}_v - \overline{U}_{sd}) - \rho_l \eta A\frac{f_{ed}}{\tau_{ed}}\Delta z(\overline{U}_v - \overline{U}_{ed}) - \alpha A\Delta z\rho_v g\sin(\Phi) = \frac{d}{dz}(\dot{m}_v U_v)\Delta z - \dot{m}_{lv}\overline{U}_{ll} \quad (7)$$

where $\tau_{sd} = \frac{\rho_l D_{sd}^2}{18\mu_v}$ and $\tau_{ed} = \frac{\rho_l D_{ed}^2}{18\mu_v}$ are the response times of the spray and entrained droplets, respectively.

3.2. Steady state one-dimensional liquid layer momentum equation

Within the liquid layer, it is assumed that the entrained droplets leave the liquid layer and enter the vapor phase at the liquid

Table 1
Contributions of momentum rate for different components shown in the control volume (Fig. 3). The two-phase flow in the mesochannel consists of four components: vapor phase, liquid layer, spray droplet and entrained droplet.

Component	Momentum inflow rate	Momentum outflow rate	Change of momentum storage rate due to transfer among components
Vapor phase	$\dot{m}_v U_v$	$\dot{m}_v U_v + \frac{d}{dz}(\dot{m}_v U_v)\Delta z$	$-\dot{m}_{lv}\overline{U}_{ll}$
Spray droplet	$\dot{m}_{sd} U_{sd}$	$\dot{m}_{sd} U_{sd} + \frac{d}{dz}(\dot{m}_{sd} U_{sd})\Delta z$	$\dot{m}_{dep,sd}\overline{U}_{sd}$
Entrained droplet	$\dot{m}_{ed} U_{ed}$	$\dot{m}_{ed} U_{ed} + \frac{d}{dz}(\dot{m}_{ed} U_{ed})\Delta z$	$\dot{m}_{dep,ed}\overline{U}_{ed} - \dot{m}_{ent,ed}\overline{U}_{ll}$
Liquid layer	$\dot{m}_{ll} U_{ll}$	$\dot{m}_{ll} U_{ll} + \frac{d}{dz}(\dot{m}_{ll} U_{ll})\Delta z$	$\dot{m}_{lv}\overline{U}_{ll} - \dot{m}_{dep,sd}\overline{U}_{sd} - \dot{m}_{dep,ed}\overline{U}_{ed} + \dot{m}_{ent,ed}\overline{U}_{ll}$

layer velocity, but the entrained droplets are deposited on liquid layer at some higher velocity. Equating the rate of change of momentum of the liquid layer to the sum of the forces on the liquid layer control volume is

$$\sum F_{ll} = \dot{m}_{ll} U_{ll} + \frac{d}{dz}(\dot{m}_{ll} U_{ll})\Delta z + \dot{m}_{ent,ed}\overline{U}_{ll} - \dot{m}_{dep,sd}\overline{U}_{sd} - \dot{m}_{dep,ed}\overline{U}_{ed} - \dot{m}_{ll} U_{ll} + \dot{m}_{lv}\overline{U}_{ll} \quad (8)$$

Using Eq. (2), the momentum equation for the liquid layer can be presented as

$$-\Delta(pA_{ll}) + \overline{p}\Delta A_{ll} - F_{l\to w} - F_{l\to i} - \forall_{ll}\rho_l g\sin(\Phi) = \frac{d}{dz}(\dot{m}_{ll} U_{ll})\Delta z + \dot{m}_{ent,ed}\overline{U}_{ll} - \dot{m}_{dep,sd}\overline{U}_{sd} - \dot{m}_{dep,ed}\overline{U}_{ed} + \dot{m}_{lv}\overline{U}_{ll} \quad (9)$$

Noting that $\forall_{ll} = A_{ll}\Delta z = \beta A\Delta z$ is the total volume of the liquid layer within the flow, then

$$-\Delta(p\beta A) + \overline{p}\Delta(\beta A) - F_{l\to w} - F_{l\to i} - \beta A\Delta z\rho_l g\sin(\Phi) = \frac{d}{dz}(\dot{m}_{ll} U_{ll})\Delta z + \dot{m}_{ent,ed}\overline{U}_{ll} - \dot{m}_{dep,sd}\overline{U}_{sd} - \dot{m}_{dep,ed}\overline{U}_{ed} + \dot{m}_{lv}\overline{U}_{ll} \quad (10)$$

The above Eq. (10) describes the rate of change of momentum in the liquid layer for non-equilibrium flows, i.e. flows with entrainment and phase change (Govan et al., 1988; Barbosa, 2005).

The governing equations for droplets are split up into two equations for ease of modeling since the velocities, and droplet sizes are different between the spray and entrained droplets.

3.3. Steady state one-dimensional spray droplet momentum equation

The spray droplet momentum equation can be derived based on the momentum model described by Kays and Crawford (1993). An Eulerian model is used (as opposed to Lagrangian) with the assumption that the droplet cloud within the channel can be treated as a continuous medium (Crowe et al., 1998). For saturated conditions, it is assumed that no mass transfer occurs between the vapor and the spray droplets, then:

$$\sum F_{sd} = \dot{m}_{sd} U_{sd} + \frac{d}{dz}(\dot{m}_{sd} U_{sd})\Delta z - \dot{m}_{sd} U_{sd} + \dot{m}_{dep,sd}\overline{U}_{sd} \quad (11)$$

Substituting Eq. (3) into Eq. (11) for the summation of forces yields

$$-3\pi N_{sd}\mu_v D_{sd} f_{sd}(\overline{U}_{sd} - \overline{U}_v) - N_{sd}\overline{\forall}_{sd}\frac{dp}{dz} - N_{sd}\overline{\forall}_{sd}\rho_l g\sin(\Phi) = \frac{d}{dz}(\dot{m}_{sd} U_{sd})\Delta z + \dot{m}_{dep,sd}\overline{U}_{sd} \quad (12)$$

The total volume of spray droplets can be expressed as $N_{sd}\overline{\forall}_{sd} = A_{sd}\Delta z = \kappa A\Delta z$. Rearranging terms, the final form of the spray droplet momentum Eq. (12) is then shown to be

$$-\rho_l\kappa A\frac{f_{sd}}{\tau_{sd}}\Delta z(\overline{U}_{sd} - \overline{U}_v) - \Delta(p\kappa A) + \overline{p}\Delta(\kappa A) - \rho_l\kappa A\Delta z g\sin(\Phi) = \frac{d}{dz}(\dot{m}_{sd} U_{sd})\Delta z + \dot{m}_{dep,sd}\overline{U}_{sd} \quad (13)$$

The equation for the spray droplet velocity can be determined from the above equation. The spray droplet mass flow rate is related to the volume fraction (κ) and the velocity (U_{sd}). By applying mass conservation laws to the spray droplets, the spray droplet velocity equation is shown to be (Schwarzkopf, 2005)

$$\Delta U_{sd}^2 = -2\frac{f_{sd}}{\tau_{sd}}\Delta z(\overline{U}_{sd} - \overline{U}_v) - 2\frac{1}{\rho_l}\Delta p - 2g\Delta z\sin(\Phi) \quad (14)$$

3.4. Steady state one-dimensional entrained droplet momentum equation

The same process outlined in the spray droplet momentum equation is used to determine the momentum equation for the entrained droplet as

$$\sum F_{ed} = \dot{m}_{ed} U_{ed} + \frac{d}{dz}(\dot{m}_{ed} U_{ed})\Delta z - \dot{m}_{ed} U_{ed} - \dot{m}_{ent,ed}\overline{U}_{ll} + \dot{m}_{dep,ed}\overline{U}_{ed} \quad (15)$$

Substituting Eq. (4) into Eq. (15) for the summation of forces acting on the entrained droplets yields

$$-3\pi N_{ed}\mu_v D_{ed} f_{ed}(\overline{U}_{ed} - \overline{U}_v) - N_{ed}\overline{\forall}_{ed}\frac{dp}{dz} - N_{ed}\overline{\forall}_{ed}\rho_l g\sin(\Phi) = \frac{d}{dz}(\dot{m}_{ed} U_{ed})\Delta z - \dot{m}_{ent,ed}\overline{U}_{ll} + \dot{m}_{dep,ed}\overline{U}_{ed} \quad (16)$$

The total volume of entrained droplets can be expressed as $N_{ed}\overline{\forall}_{ed} = A_{ed}\Delta z = \eta A\Delta z$. The entrained droplet momentum Eq. (16) is then rearranged to show

$$-\rho_l\eta A\frac{f_{ed}}{\tau_{ed}}\Delta z(\overline{U}_{ed} - \overline{U}_v) - \Delta(p\eta A) + \overline{p}\Delta(\eta A) - \eta\rho_l A\Delta z g\sin(\Phi) = \frac{d}{dz}(\dot{m}_{ed} U_{ed})\Delta z - \dot{m}_{ent,ed}\overline{U}_{ll} + \dot{m}_{dep,ed}\overline{U}_{ed} \quad (17)$$

The equation for the entrained droplet velocity can be determined from the above equation. The entrained droplet mass flow rate is related to the entrained droplet volume fraction (η) and the entrained droplet velocity (U_{ed}). Applying mass conservation laws to the entrained droplets, the velocity equation for the entrained droplet is shown to be (Schwarzkopf, 2005)

$$\Delta U_{ed}^2 = -2\frac{f_{ed}}{\tau_{ed}}\Delta z(\overline{U}_{ed} - \overline{U}_v) - 2\frac{1}{\rho_l}\Delta p - 2g\Delta z\sin(\Phi) - \frac{2\dot{m}_{ent}\Delta z}{N_{ed}\rho_l\frac{\pi}{6}D_{ed}^3}(\overline{U}_{ed} - \overline{U}_{ll}) \quad (18)$$

3.5. Steady State one-dimensional two-phase momentum equation

The two-phase flow considered in Fig. 3 consists of four components; the momentum equation for the system can be obtained by summing the individual equations for each component (i.e. Eqs. (7), (10), (13), and (17))

$$-\Delta(pA(\alpha+\beta+\kappa+\eta)) + \overline{p}\Delta((\alpha+\beta+\kappa+\eta)A) - [\alpha\rho_v + \rho_l(\beta+\kappa+\eta)]A\Delta z g\sin(\Phi) - F_{v\to w} - F_{l\to w} - F_{l\to i} - F_{v\to i} = \Delta(\dot{m}_v U_v + \dot{m}_{ll} U_{ll} + \dot{m}_{sd} U_{sd} + \dot{m}_{ed} U_{ed}) \quad (19)$$

The liquid and vapor interfacial forces are equal due to the no slip and no penetration condition (i.e. $F_{v\to i} = -F_{l\to i}$) and the sum of the individual volume fractions must equate to the total volume (i.e. $\alpha + \beta + \kappa + \eta = 1$). Applying these relationships to Eq. (19) yields

$$-\Delta(pA) + \overline{p}\Delta(A) - \left[\alpha\rho_v + \rho_l(1-\alpha)\right]A\Delta z g\sin(\Phi) - F_{v\to w} - F_{l\to w} = \Delta(\dot{m}_v U_v + \dot{m}_{ll}U_{ll} + \dot{m}_{sd}U_{sd} + \dot{m}_{ed}U_{ed}) \quad (20)$$

Here, a fictitious two-phase pressure gradient is used to account for the combined liquid- and vapor-wall shear effects and is typically defined as (Carey, 1992)

$$F_{v\to w} + F_{l\to w} = -\left(\frac{\Delta p}{\Delta z}\right)_{fr}\overline{A}\Delta z \quad (21)$$

According to Carey (1992), a relationship exists between the total mass flux (G) and the liquid layer and vapor velocities for uniform flow. The mass flow rate of the vapor core is expressed as

$$\dot{m}_v = GAx \quad (22)$$

The average vapor velocity can be defined as

$$U_v = \frac{\dot{m}_v}{\rho_v A_v} = \frac{GAx}{\rho_v A_v} = \frac{Gx}{\alpha\rho_v} \quad (23)$$

The liquid layer mass flow can be defined in terms of the total mass flux

$$\dot{m}_{ll} = G(1-x)(1-E-S)A \quad (24)$$

where E is the liquid entrainment mass fraction and S is the liquid spray mass fraction. Utilizing Eq. (24), the average liquid layer velocity can be expressed in terms of the total mass flux as

$$U_{ll} = \frac{\dot{m}_{ll}}{\rho_l A_{ll}} = \frac{G(1-x)(1-E-S)A}{\rho_l A_{ll}} = \frac{G(1-x)(1-E-S)}{\rho_l\beta} \quad (25)$$

The mass flow rate of the spray droplets and the entrained droplets can be represented by

$$\dot{m}_{sd} = GA(1-x)S = \kappa\rho_l A U_{sd} \quad (26)$$

$$\dot{m}_{ed} = GA(1-x)E = \eta\rho_l A U_{ed} \quad (27)$$

Substituting Eqs. (21)–(27) into the two-phase momentum Eq. (20) yields

$$-\frac{dp}{dz} + \left(\frac{dp}{dz}\right)_{fr} - g\sin(\Phi)(\alpha\rho_v + (1-\alpha)\rho_l) = \frac{1}{\overline{A}}\frac{d}{dz}\left[\alpha\rho_v A\left(\frac{Gx}{\alpha\rho_v}\right)^2 + \beta\rho_l A\left(\frac{G(1-x)(1-E-S)}{\rho_l\beta}\right)^2 + \kappa\rho_l A U_{sd}^2 + \eta\rho_l A U_{ed}^2\right] \quad (28)$$

Eq. (28) represents the change in pressure of the bulk stream, consisting of spray droplets, entrained droplets, a liquid layer, and a vapor core. The spray and entrained droplet velocities are given by Eqs. (14) and (18), respectively. These are solved using an iteration technique (described in Numerical Techniques section). Currently, the two-phase friction term, the volume fractions, and the entrainment mass fraction are unknown. To close the equation set, a few constitutive relationships are needed.

3.6. Constitutive relationships

Traditionally, the two-phase friction term is empirically modeled as

$$\left(\frac{dp}{dz}\right)_{fr} = \phi_v^2\left(\frac{dp}{dz}\right)_v \quad (29)$$

The single phase turbulent-vapor only pressure gradient $(dp/dz)_v$ and ϕ_v^2 (two-phase multiplier) can be modeled by the methods described in Carey (1992). An empirical correlation for the void fraction (α) was determined by Butterworth (1975)

$$\alpha = \frac{1}{1 + 0.28X^{0.71}} \quad (30)$$

where X is the Martinelli factor (Lockhart and Martinelli, 1949). In Eq. (30), the Martinelli factor (X) is replaced by the turbulent-liquid–turbulent-vapor Martinelli factor (X_{tt}) defined as (Carey, 1992)

$$X_{tt} = \left(\frac{\rho_v}{\rho_l}\right)^{0.5}\left(\frac{\mu_l}{\mu_v}\right)^{0.125}\left[\frac{1-x}{x}\right]^{0.875} \quad (31)$$

The spray droplet volume fraction (κ), and the entrained droplet volume fraction (η) can be presented in terms of mass flux as

$$\kappa = \frac{GA(1-x)S}{\rho_l A U_{sd}} \quad (32)$$

$$\eta = \frac{GA(1-x)E}{\rho_l A U_{ed}} \quad (33)$$

Knowing that the volume fractions of each component must sum to unity, the liquid layer volume fraction (β) can be determined by the relation

$$\beta = 1 - \alpha - \kappa - \eta \quad (34)$$

3.7. Entrainment terms

The entrainment droplet diameter can be estimated using the empirical relation proposed by Ueda (1981)

$$D_{ed} = 0.0058\left[\left(\frac{\sigma}{\mu_v U_v}\right)\left(\frac{\rho_v}{\rho_l}\right)^{1.25}\right]^{0.34} D_t \quad (35)$$

Owen and Hewitt (1986) proposed a relation for the minimum liquid mass flux (G_{lfo}) at which entrainment will occur. If the liquid layer mass flux is greater than the minimum liquid mass flux, entrainment will occur (Carey, 1992). If entrainment occurs, then the mass fraction of entrained droplets is needed. Govan et al. (1988) relates the entrainment mass fraction to the entrained droplet mass concentration (C), from which the entrainment mass fraction can be expressed as

$$E = \frac{Cx}{\rho_v(1-x)(1-\frac{C}{\rho_l})} \quad (36)$$

The entrained droplet mass concentration (C) for equilibrium flow was empirically determined by Govan et al. (1988). The correlation proposed by Govan et al. (1988) was modified to account for the spray mass fraction and is shown as

$$C = 0.0000575\left(\frac{Gx}{k_d}\right)(G(1-x)(1-E-S) - G_{lfo})^2\left(\frac{D_t\rho_l}{\sigma\rho_v^2}\right)^{0.316} \quad (37)$$

The entrained droplet deposition coefficient (k_d) is also proposed by Govan et al. (1988) as

$$k_d\sqrt{\frac{\rho_v D}{\sigma}} = 0.18 \quad \text{if } \frac{C}{\rho_v} < 0.3 \quad (38)$$

$$k_d\sqrt{\frac{\rho_v D}{\sigma}} = 0.083\left(\frac{C}{\rho_v}\right)^{-0.65} \quad \text{if } \frac{C}{\rho_v} \geqslant 0.3 \quad (39)$$

The above entrainment correlations are for vertical annular flow. Here it is assumed (based on the work of Gersey and Mudawar (1992)) that if the flow is annular in mesoscale channels, the gravitational effect is minimal, thus horizontal applications should be

valid. It is also assumed that the correlation for concentration applies to Fluorinert™. Although Eqs. (37)–(39) are correlated with data for equilibrium flow, these correlations were assumed to be valid in predicting non-equilibrium flows (the reader is referred to Govan et al. (1988) for further details).

4. Experimental setup

A picture of the setup showing the tube sizes is shown in Fig. 4a. Eight stainless steel tubes (0.12 cm internal diameter) were installed and sealed with epoxy, three of which were used to measure reference pressures and five placed within the channel. Polymer tubing was then installed on the stainless steel tubes and routed to a manifold which allowed a transition in tubing size. The tubing was then run to a differential pressure transducer (Omega Model PX2300-1DI). The range of the pressure transducer was 0 - 6,895 Pa, with an accuracy of 17.2 Pa; this was the best measurement device found that contained materials that were compatible with PF5050. Care was taken to make sure the pressure transducer ports and the manifold were at the same height as the ports in the spray module and that the lines were as short as possible to minimize uncertainty caused by fluid condensing in the lines.

Fig. 4b and c shows a schematic of the overall experimental setup. The data acquisition system was a Keithley 2700 with a 7708 module. A thin film Kapton heater was carefully placed over the finned area of the spray module base. The voltage and current (using a shunt) supplied to the heater were measured by the Keithley. The heater input power was limited to 100 W to avoid pressure oscillation. The pressure at the inlet and exit ports of the spray module was measured with SenSym SCX100ANC pressure trans-

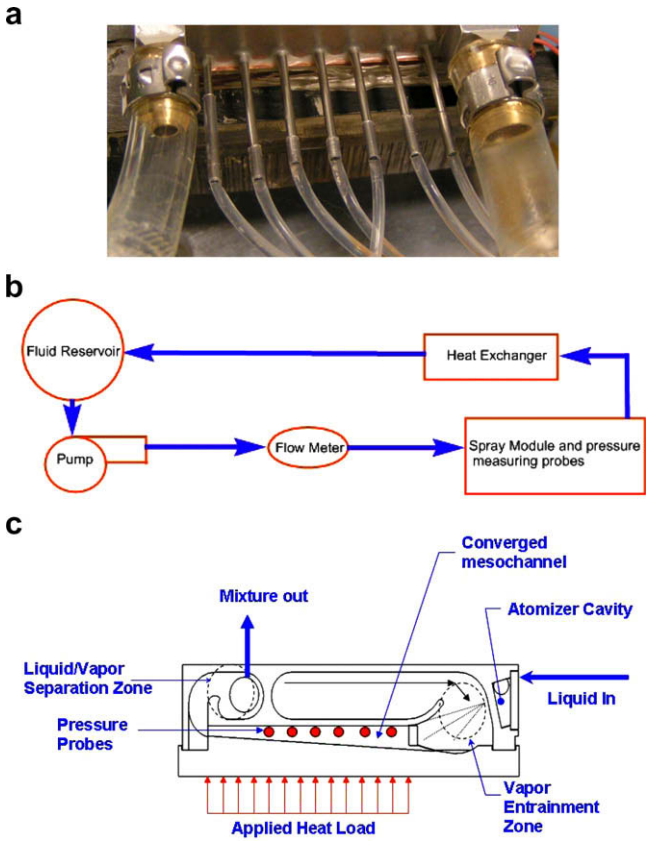

Fig. 4. (a) Photograph of the experimental setup. (b) Schematic of the experimental setup used in this study and (c) exploded view of the spray module.

Table 2
Values used to evaluate pressure drop in the channel.

Spray droplet diameter (D_{sd}), μm	20
Spray droplet velocity (U_{sd}), m/s	8
Liquid spray mass fraction (S)	0.2
Channel wall angles (δ, χ), °	3.1, 0
Liquid mass flow rate ($\dot{m}_{sd} + \dot{m}_{ll}$), kg/s	0.0024
Initial quality (x_i)	9.8%
Channel length (z), cm	3.43
Channel inlet hydraulic diameter (D_t), mm	1.55
Channel exit hydraulic diameter (D_t), mm	1.17
Saturation temperature, °C	34
Spray mass deposition ($\dot{m}_{dep,sd}$), kg/s	0
Fluid type	PF5050

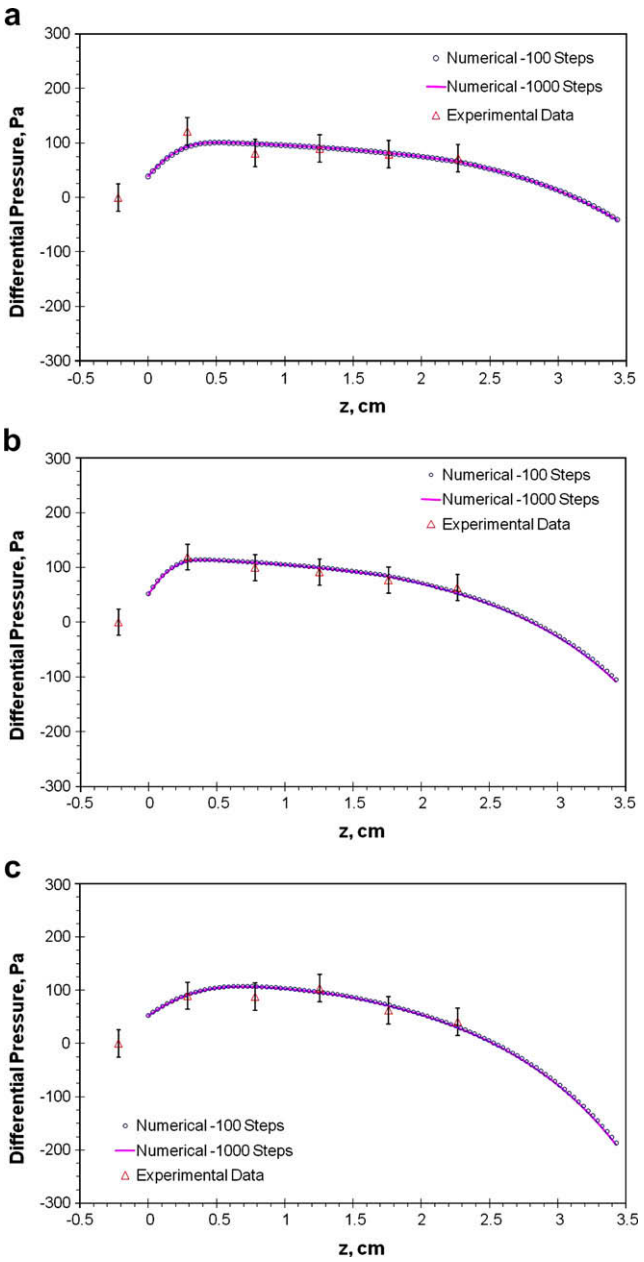

Fig. 5. Comparison of model prediction to experimental measurement for (a) 50 W, (b) 75 W and (c) 100 W. All other simulation conditions are presented in Table 2. For all experimental cases, the reference pressure was measured by providing a pressure probe at the upstream of the channel. Five pressure probes were located in the channel region.

ducers and recorded with the Keithley. The flow rate was measured upstream of the atomizers with a McMillan 102-4T turbine flow meter and also recorded by the Keithley. The heat exchanger is a Lytron ES505 with a Galaxy Fan; the air temperature at the inlet of the heat exchanger was measured at 21 °C. The heat exchanger and reservoir were elevated approximately one meter above the spray module and pump to prevent cavitation at the pump inlet. The saturation temperature measured at the exit of the module was 34 °C. The pressure difference across the atomizers was fixed to produce a liquid mass flow rate of 0.0024 kg/s. Details of the spray module are described elsewhere (Schwarzkopf et al., 2005).

5. Numerical techniques

A numerical algorithm is developed to estimate the two-phase pressure along the channel. Table 2 shows the boundary conditions and selected parameters that were used in the modeling. At the channel inlet boundary, three parameters, namely the spray droplet diameter, spray droplet velocity and the liquid spray mass fraction, were unknown. The spray droplet velocity at the channel inlet boundary was estimated from a numerical model developed elsewhere (Schwarzkopf, 2005), and the spray droplet diameter and spray mass fraction was iterated until the pressure at the onset of the channel matched the interpolated results of the experimental data. Although the values for the spray droplet diameter and velocity (shown in Table 2) were not directly measured, they appear to be in reasonable agreement with the atomization data collected by a phase Doppler interferometer (PDI), (Schwarzkopf, 2006). The numerical algorithm used to solve pressure is similar to the standard explicit scheme where the pressure at the $(i+1)$th step is calculated based on known information at the ith step. A pressure at the $(i+1)$th step is guessed to calculate the change in velocity of the spray and entrained droplets at the $(i+1)$th step. The two-phase pressure is then calculated from Eq. (28). The residual is determined as the difference between the guessed value and the calculated value. The residual is used with a relaxation factor to adjust the guessed pressure for the next iteration. The iterations continue until the calculated pressure at each step converges to within 10^{-3} Pa of the guessed pressure. Since the explicit algorithm relies on very small step sizes, the number of steps was increased by 10x to ensure the solution remained the same.

Fig. 5 shows the pressure distribution along the channel based on the selected parameters listed in Table 2. Each figure is identified with a heat load which controls the quality within the channels. The quality was determined by an energy balance across the computational cell. For a uniform heat load, the heat was divided into N number of cells. In any flow study, the conservation of mass and momentum is of paramount interest. In this numerical work, the mass conservation is checked by

$$\left|\frac{(\alpha\rho_v U_v + \beta\rho_l U_{ll} + \kappa\rho_l U_{sd} + \eta\rho_l U_{ed})_i A_i - \dot{m}_{int}}{\dot{m}_{int}}\right| \times 100\%$$

where $\dot{m}_{int}$ is the initial mass flow rate. The momentum conservation is tested by

$$\left|\frac{\left[\sum_{n=1}^{4}\dot{m}_n U_n\right]_{i+1} - \left[\sum_{n=1}^{4}\dot{m}_n U_n\right]_i + P_{i+1}A_{i+1} - P_i A_i + \frac{1}{2}(P_{i+1}+P_i)(A_i - A_{i+1})}{\frac{1}{4}(P_{i+1}+P_i)(A_i + A_{i+1})}\right| \times 100\%$$

where n represents the component (i.e. vapor, liquid layer, spray droplet, entrained droplet).

The conservation of mass flow rate showed to be less than 0.01% throughout the channel for all heat loads (50 W, 75 W and 100 W), while the momentum was conserved within 0.2% throughout the channel. In addition, the step size was varied by an order of magnitude to ensure grid independent results. To validate our quasi-one-dimensional numerical model, experimental results are also shown for identical flow and thermal conditions. The error bars in experimental results show the RMS variation. The trend and magnitude of the numerical prediction (Fig. 5a–c) fit within the experimental uncertainty (17.2 Pa).

6. Results and discussion

A comparison of the numerical model and the experimental data is shown in Fig. 5. The data collected show that for constant atomization conditions, the increased heat load causes a change in the pressure gradient. In addition, the peak pressure point is shifted downstream. Traditional two-phase pressure drop formulations, such as those given by stratified or homogeneous flow theory (Carey, 1992), would predict a negative pressure gradient for this type of channel geometry. However, the trend of the numerical model (shown in Fig. 5) shows a positive pressure gradient that transition to a negative pressure gradient, in agreement with the data. The positive pressure gradient at the entry region is explained by the atomized droplets initially having a higher velocity than the surrounding vapor. In this region, the atomized droplets act as a pump by transferring momentum to the surrounding vapor. The negative pressure gradient is explained by the velocity of the vapor being higher than the velocity of the other components due to boiling. In this region, vapor momentum is increasing due to vapor generation caused by boiling and the atomized droplets are being pumped.

The predicted velocity profiles for each component of the two-phase fluid are shown in Fig. 6 for the 100 W case. Comparing Figs. 5c to 6, the transition from a positive to a negative pressure gradient occurs when the spray velocity approaches the vapor velocity. Thus the positive pressure gradient shown in Fig. 5c occurs due to the droplet drag effects on flowing vapor. The magnitude of the drag effects depends on the relative velocity between the phases. The response time of the droplets coupled with the increase in vapor mass flow and the change in cross-sectional area prevents the droplets from reaching the vapor velocity. This non-equilibrium effect is responsible for producing the negative pressure gradient. But, even while the flow is in a non-equilibrium state, if the droplet diameter, initial spray mass fraction and velocity were changed at the channel inlet, the channel geometry could be optimized to minimize the negative pressure gradient. The entrained droplets will always produce a negative pressure gradient in the fluid stream because they enter the vapor core at the liquid layer velocity and undergo acceleration. The effects of entrained droplets on pressure is less than 1% relative to flows with no entrained droplets for low initial qualities ($x_i \leqslant 0.2$) and mass flow rates as shown in Fig. 7.

Although the momentum effects of entrained droplets show insignificant contributions to the pressure distribution, the entrained droplets do have a moderate effect on the liquid layer mass flow rate (shown in Fig. 8). The liquid layer mass flow rate decreases due to mass transfer from the liquid layer to the vapor core through phase change and entrained droplets. Knowing the magnitude of mass that is transferred, action can be taken to prevent premature dry out. In addition, these results could aid in the

development of a non-uniform spray pattern that could be used with the correct geometry design to deposit spray droplets at the rate of entrainment throughout the channel length for non-equilibrium multi-phase flows. It can also provide insight into alternative methods such as feeding the channels with the appropriate liquid mass flow rate (i.e. a liquid source) at a specific point in the channel. The numerical model could be easily adapted to incorporate such ideas.

After validating the model, a few case studies are presented. Even though this model is able to predict the pressure distribution along the channel for a number of parameters, the effects of channel wall angle, spray mass fraction, and droplet velocity are studied because of their relative importance. The nominal values for each parameter studied are reflected in Table 2. A higher relative pressure at the channel exit is optimal in producing a vapor source that will allow a net amount of vapor to be transported from the high pressure exhaust region to the low pressure vapor entrainment region, near the spray cones. In addition, the vapor momentum flux

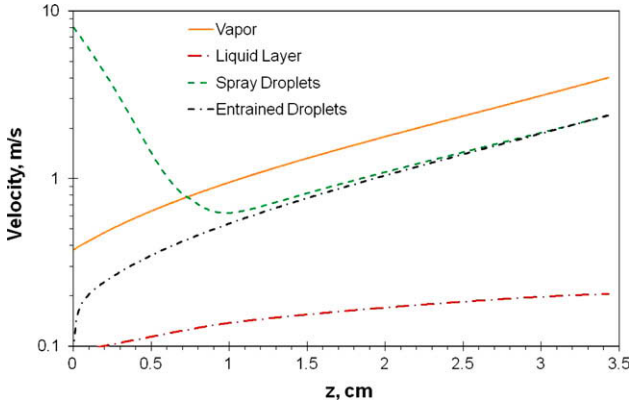

Fig. 6. Velocity profile of different components along the channel for the 100 W case. Other simulation conditions are the same as Fig. 5.

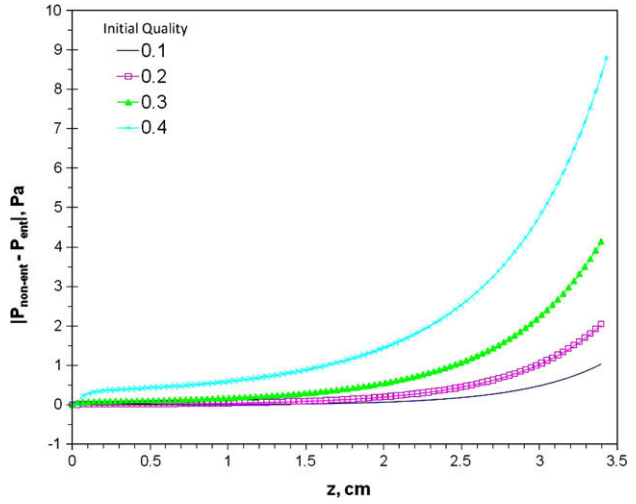

Fig. 7. Effect of entrainment on pressure distribution for 100 W case. Other simulation conditions are the same as Fig. 5.

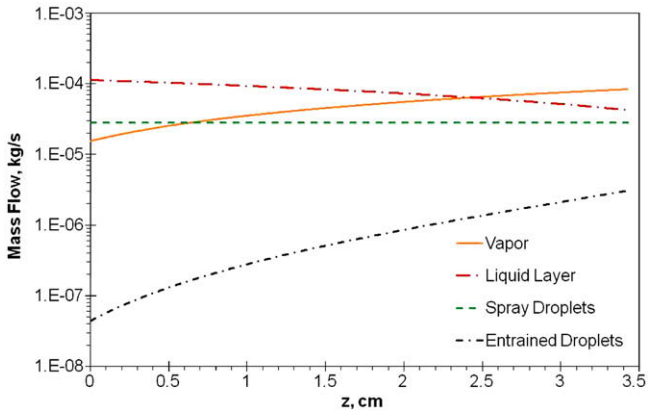

Fig. 8. Mass flow rate distribution of different components along the channel for the 100 W case. Other simulation conditions are the same as Fig. 5.

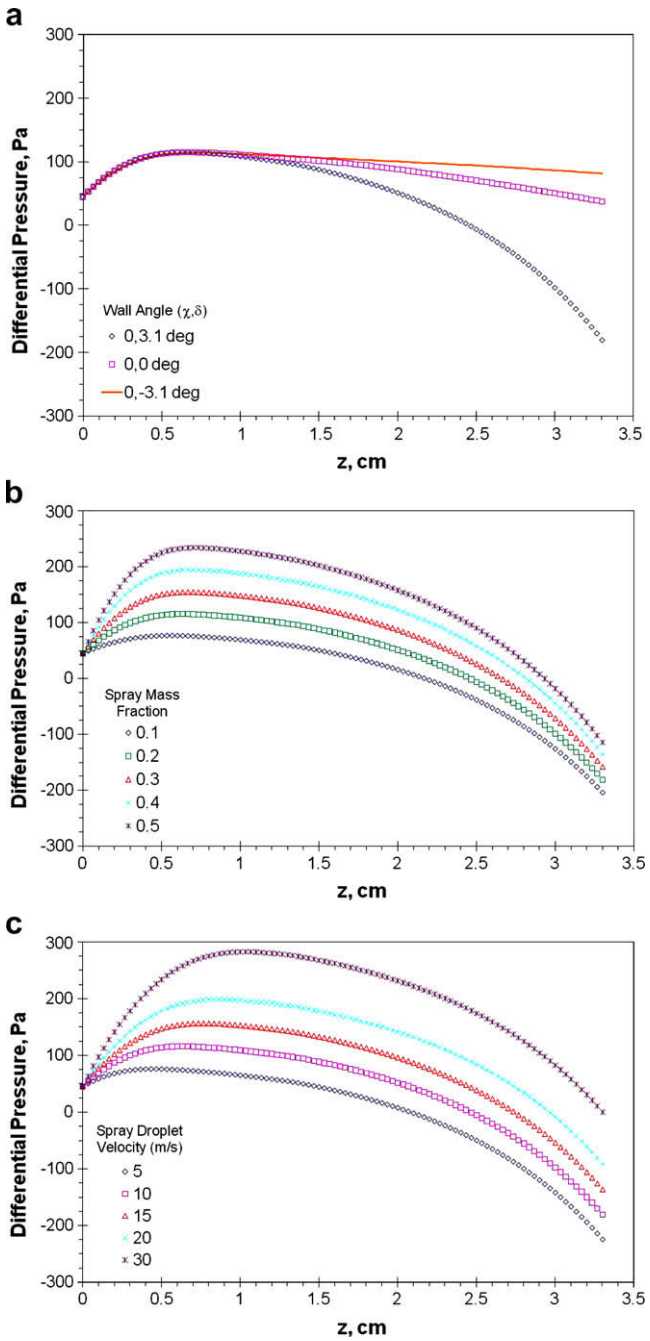

Fig. 9. Effects of (a) channel wall angle (b) spray mass fraction, and (c) droplet velocity on pressure distribution for the 100 W case.

at the onset of the channel must be greater than the pressure gradient within the channel. This flux is typically low, thus a minimal pressure difference across the channel is required. If the flow axis is horizontal ($\Phi = 0^\circ$), a potential pressure gain at the channel exit can be achieved by changing the channel wall angle as shown in Fig. 9a, where $\chi = 0^\circ$ and $\delta = 0^\circ$ is a straight channel, $\chi = 0^\circ$ and $\delta = 3.1^\circ$ is a converging channel, and $\chi = 0^\circ$ and $\delta = -3.1^\circ$ is a diverging channel. Another method of increasing the pressure at the channel exit is to increase the spray mass fraction while maintaining the same overall mass flow rate. The model shows that a higher spray mass fraction will also aid in increasing the relative pressure at the channel exit (Fig. 9b). In addition, if the velocity of the droplets were increased at the onset of the channel, the pressure at the exit of the channel is increased (Fig. 9c). It is also shown that the peak pressure point is shifted within the channel by increasing the spray mass fraction or initial droplet velocity (Fig. 9b and c). This shift is due to the conditions at the onset of the channel and is different than the shift shown in Fig. 5a–c, which is due to increased boiling. The shift shown in Fig. 9b and c is a good indication that the vapor momentum flux is adequate to overcome the pressure gradient due to boiling. These, combined with wall angles of $\chi = 0^\circ$ and $\delta = -3.1^\circ$, suggest that a higher quality throughout the channel can be achieved, thereby increasing the overall heat transfer in a low profile setting.

7. Conclusions

A pseudo one-dimensional numerical model was developed for two-phase flow in a converging mesochannel with phase change due to the heat acquisition from an external source and an initial quality supplied by an atomization process. The model accounted for effects of sprayed droplets, entrained droplets, liquid layer on the wall, and a vapor core in the center of the mesochannel. An explicit numerical scheme is used to obtain pressure distribution along the channel from the model equation. In the numerical scheme, the overall conservation of mass was less than 0.01% and overall conservation of momentum was less than 0.2%.

An experiment was developed to measure the two-phase pressure drop within the channels; the fluid was a dielectric solvent - PF5050. The predictions of the pseudo one-dimensional numerical model show qualitative agreement with the measured trends of pressure distribution. The entrainment droplets have negligible effects in the overall momentum transport, but their contribution decreases the mass flow rate of the liquid layer which can lead to dryout conditions. For low initial quality, the pressure difference between entrainment and no-entrainment case is less than 1%. Unlike the trends predicted by homogeneous or stratified flow theory, a positive pressure gradient is observed at the entry section due to the atomized droplets having a higher velocity than the vapor. The positive pressure gradient at the entry region shifts the location of maximum pressure point from the onset of the channel to some point downstream.

Finally, the effects of channel wall angle, spray mass fraction, and spray droplet velocity are considered in relation to the pressure performance within the mesochannel. For the 100 W case, the numerical model predicts a higher relative pressure at the channel exit for the diverging channel when compared to the converging or straight channel. This optimal setting will aid in the transport of vapor from the high pressure exhaust region to the low pressure vapor entrainment region near the spray cones. It will also allow vapor to be pumped into the channels and highlights areas to consider when designing such a device for high heat flux environments.

Acknowledgements

Support of this work was provided by Isothermal Systems Research Inc., Research and Development Department, Pullman, WA. A special thanks to Mr. Charles Tilton and Dr. Don Tilton for many valuable discussions.

References

Barbosa Jr., J.R., 2005. Two-phase non-equilibrium models: the challenge of improving phase-change heat transfer prediction. J. Braz. Soc. Mech. Sci. Eng. 27 (1), 31–45.

Butterworth, D., 1975. A comparison of some void-fraction relationships for co-current gas–liquid flow. Int. J. Multiphase Flow 1 (6), 845–850.

Cader, T., Tilton, D., 2004. Implementing spray cooling thermal management in high heat flux applications. In: ITHERM, June, 2004, Las Vegas, NV.

Carey, V.P., 1992. Liquid–Vapor Phase-Change Phenomena. Hemisphere Publishing Corporation, New York.

Chen, J.C., 1966. A correlation for boiling heat transfer to saturated fluids in convective flow. Ind. Eng. Chem.: Process Des. Develop. 5 (3), 322–329.

Chu, R.C., Simons, R.E., Ellsworth, M.J., Schmidt, R.R., Cozzolino, V., 2004. Review of cooling technologies for computer products. IEEE Trans. Dev. Mat. Reliab. 4 (4), 568–585.

Crowe, C.T., Sommerfeld, M., Tsuji, Y., 1998. Multiphase Flows with Droplets and Particles. CRC Press LLC, Boca Raton, Florida, USA.

Gersey, C.O., Mudawar, I., 1992. Effects of orientation on critical heat flux from chip arrays during flow boiling. J. Electron. Packag. 114, 290–299.

Govan, A.H., Hewitt, G.F., Owen, D.G., Bott, T.R., 1988. An improved CHF modelling code. In: Proc. Second UK National Heat Transfer Conference, London, UK, pp. 33–48.

Kays, W.M., Crawford, M.E., 1993. Convective Heat and Mass Transfer. McGraw Hill, New York.

Lockhart, R.W., Martinelli, R.C., 1949. Proposed correlation of data for isothermal two-phase, two-component flow in pipes. Chem. Eng. Progress. 45 (1), 39–48.

Mudawar, I., Estes, K.A., 1996. Optimizing and predicting CHF in spray cooling of a square surface. J. Heat Transfer 118, 672–679.

Owen, D.G., Hewitt, G.F., 1986. A Proposed Entrainment Correlation, AERE-R12279.

Rini, D.P., Chen, R.H., Chow, L.C., 2001. Bubble behavior and heat transfer mechanism in FC-72 pool boiling. Exp. Heat Transfer 14 (1), 27–44.

Rini, D.P., Chen, R.H., Chow, L.C., 2002. Bubble behavior and nucleate boiling heat transfer in saturated FC-72 spray cooling. J. Heat Transfer 124, 63–72.

Schwarzkopf, J.D., Tilton, C.L., Crowe, C.T., Li, B.Q., 2005. A low profile thermal management device for high power processors using enhanced flow boiling techniques and perfluorocarbon fluids. In: ASME Summer Heat Transfer Proceedings, San Francisco, CA, June 2005.

Schwarzkopf, J.D., 2005. A Numerical Study of Enhanced Flow Boiling Techniques for Multi-Phase Narrow Channel Flows using Liquid Atomization. M.S. Thesis, Washington State University, Pullman, WA.

Schwarzkopf, J.D., 2006. Atomization Performance Comparison of the Original Brass to the New Welded Acetyl Injection Molded Atomizers. Isothermal Systems Research Inc., Report ATM-2006-008-1.

Tilton, D.E., 1989. Spray Cooling. Ph.D. Dissertation. University of Kentucky, Lexington, KY.

Ueda, T., 1981. Annular and mist flow. In: Bergles, A.E., Ishigai, Seikan (Eds.), Two Phase Flow Dynamics. Hemisphere Publishing Corporation, NY, pp. 75–94.